Journal of the European Ceramic Society **10** (1992) 1–12

Fibre-reinforced SiC-Matrix Composites: Microstructure, Interfaces and Mechanical Properties

G. Grathwohl,[a] A. Hähnel,[b] B. Meier,[a] E. Pippel,[b] G. Richter[a] & J. Woltersdorf[b]

[a] Institut für Keramik im Maschinenbau, Universität Karlsruhe, Haid- und Neu-Straße 7, W-7500 Karlsruhe, FRG
[b] Institut für Festkörperphysik und Elektronenmikroskopie Halle, Weinberg 2, 0-4050 Halle (Saale), FRG

(Received 17 July 1991; revised version received 30 September 1991; accepted 14 October 1991)

Abstract

Two fibre-reinforced SiC-materials containing SiC- and C-fibres, respectively, are characterized by evaluation of their microstructures, especially by microanalysis of the interfaces between fibre and matrix and by their mechanical properties. The interfaces show a layered structure consisting of C-layers and an intermediate SiO_2-layer in the case of C-fibre and SiC-fibre reinforced ceramics, respectively. C-layers are also found to interrupt the SiC-matrix, then discriminating the individual chemical vapour infiltration (CVI) sequences during the formation of the matrix. Both interlayer phenomena can be effective in provoking favourable pull-out processes during mechanical loading of the composites. While the C-fibre reinforced ceramic reveals an increase in strength when being tested in vacuum at elevated temperatures, the strength of the SiC-fibre reinforced ceramic decreases drastically in the high-temperature test in air, both being compared to room-temperature conditions. This loss of strength is caused by the destruction of the interfacial C-layers due to oxidation processes.

In dieser Arbeit wurden zwei verschiedene faserverstärkte SiC-Werkstoffe, jeweils mit SiC- oder C-Fasern, durch die Beschreibung ihrer Gefüge, insbesondere durch Mikroanalytik der Grenzflächen zwischen Fasern und Matrix, und durch ihre mechanischen Eigenschaften charakterisiert. Die Grenzflächen zeigen eine geschichtete Struktur, die für den Fall der C- und SiC-faserverstärkten Keramik aus C-Schichten mit eingelagerter SiO_2-Schicht aufgebaut sind. C-Schichten sind jedoch auch innerhalb der SiC-Matrix eingelagert, wodurch die individuelle CVI-Sequenz bei der Bildung der Matrix unterdrückt wird. Beide Grenzflächenphänomene können genutzt werden, um günstige 'Heraus-Zieh'-Prozesse bei mechanischer Beanspruchung der Verbunde einzuleiten. Im Vergleich zu Raumtemperaturbedingungen resultieren folgende Ergebnisse bei hohen Temperaturen. Die C-Faser verstärkten Keramiken zeigen eine Festigkeitssteigerung bei Beanspruchung unter Vakuum bei hohen Temperaturen. Die Festigkeit bei hohen Temperaturen und an Luft für die SiC-faserverstärkten Keramiken dagegen fällt drastisch ab. Diese Festigkeitseinbuße wird durch die Zerstörung der C-Zwischenschichten infolge von Oxidation verursacht.

Deux matériaux à base de SiC renforcés respectivement par des fibres de SiC et de C, sont caractérisés par l'étude de leur microstructure; en particulier par microanalyse des interfaces fibre–matrice et par leurs propriétés mécaniques. Les interfaces présentent une structure en couche constituée de couches de C et de couches de SiO_2 intermédiaries dans le cas de céramiques renforcées par des fibres de SiC, et dans le cas de fibres de C des couches de C ont aussi été trouvées, qui interrompent la matrice de SiC et ainsi séparent les séquences individuelle CVI pendant la formation de la matrice. Ces deux phénomènes d'intercouche favorisent la phénomène de pull-out lors de l'application d'une charge mécanique aux composites. Alors que les céramiques renforcées par des fibres de C présentent une augmentation de leur résistance mécanique quand elles sont testées sous vide à haute température, la résistance des céramiques renforcées par des fibres de SiC diminue de façon importante lors d'un test à haute température et à l'air; ceci en comparaison avec les propriétés à

Journal of the European Ceramic Society 0955-2219/92/$05.00

température ambiante. Cette perte de résistance mécanique est due à la destruction des couches interfaciales de C par oxidation.

1 Introduction

In general, improving the properties of ceramic materials—of monolithic as well as of fibre-reinforced ones—is realized by optimizing the microstructure. This presupposes knowledge of the correlation between the process parameters, the microstructure and the macroscopic properties. As the mechanical behaviour is essentially governed by the interface structure, i.e. the types and the distribution of internal boundaries, the analysis and optimization of interfaces are of particular importance. In recent years considerable progress has been made in developing high-performance ceramic materials by incorporating fibres of high tensile strength. Such fibre-reinforced materials seem to be most promising for fulfilling the required quasi-ductile and damage-bearing stress–strain behaviour also in the high-temperature range. In this respect, these composite materials are more striking than the usual monolithic ceramics with their established microcrack and transformation toughening mechanisms. Within the composites the following micromechanisms are used as energy-dissipative processes: debonding between fibre and matrix, crack bridging, fibre pull-out, multiple crack formation and crack deflection. It is evident that these mechanisms are controlled by interface phenomena, particularly by the special properties of the interface between fibre and matrix and the composition of interfacial layers or interphases. In general, improving the toughness demands an appropriate sliding resistance at the interface, enabling an energy-consuming friction-hindered gliding of the fibres, which can be obtained by a suitable fibre coating.

Unlike the composites with glassy matrices[1,2] materials with SiC-matrices—produced by chemical vapour infiltration (CVI) techniques[3,4]—exhibit excellent high-temperature properties. Therefore, in this particular study, two SiC-matrix composites (Refractory Composites, 'RECOMP', California, USA) containing SiC- and C-fibres, respectively, have been examined. The investigations include tensile tests at room temperature and three-point bending tests at room temperature and elevated temperatures in air and under vacuum. For a better understanding and interpretation of both the mechanical properties and the degradation effects occurring at high temperatures, the microstructure and chemical composition were characterized by employing Auger spectroscopy and different electron microscope methods. Special emphasis was laid on the correlation between the interface microstructure and the mechanical behaviour.

2 Experimental

Two composites of identical two-dimensional weave structure but with different fibres, i.e. SiC- and C-fibres, were examined. The as-received state is described in Table 1. The composites have been coated with a SiC-layer of about 200 μm in thickness. For the SiC-fibre reinforced composite the coating leads to a smooth surface, whereas for the C-fibre reinforced material it yields a surface roughness corresponding to the weave structure.

Porosity measurements were made using a water infiltration technique.[5] For three-point bending tests at room temperature an Instron 1362 testing machine was used with typical specimen dimensions length l, width w and height h of 170 mm × 10 mm × 5 (or 6) mm and the fibres oriented parallel to the l and w directions, the span to height ratio (l/h) being larger than 25 (load control: 10 N/s). At elevated temperatures the three-point bending tests were performed in Instron machines at a constant cross-head speed of 0·01 mm/s (Type 1362 for testing the SiC-fibre reinforced composite in air, and Type 8062 for testing the C-fibre reinforced composite under vacuum). The specimen dimensions for these inves-

Table 1. Composites in the as-received state

Reinforcing component	*Dimensions of the plates (mm)*			*Number of layers*	*Number of fibre per bundle*	*Fibre type*	*Mean fibre diameter (μm)*	*Fabric* weave*
	Length	*Width*	*Thickness*					
SiC-fibre	200	100	5	15	500	Nicalon*	15	8 harness satin
C-fibre	200	100	6	10	3000	T 300	7	8 harness satin

* Producer information.

tigations were 100 mm × 8 mm × 5 (or 6) mm with $l/h > 14$. From rectangular beams tensile specimens were prepared having the dimensions 140 mm × 8 mm × 5 (or 6) mm, with the width in the gauge length of the tensile specimens being reduced from 8 to 5 mm. At their ends the samples were adhesively bonded with Al tabs, each being about 50 mm long. The transition between these end parts of the tensile specimens and the gauge length was provided by a radius of 70 mm, leaving 20 mm as the test gauge length.

For optical microscopy a Zeiss microscope was used. X-Ray investigations were performed in a Siemens D500 diffractometer applying Cu $K_{\alpha 1}$ irradiation. For this purpose, the samples were powdered to particle sizes smaller than 20 μm to reduce any preferred orientation, absorption and particle size effects. A scanning electron microscope (JEOL, Type JSM 840) equipped with an energy dispersive analyser (Kevex quantum detector) was employed for microstructural observations. High-resolution Auger electron spectroscopy (HRAES) was carried out using a Perkin Elmer (PHI 600) instrument. Typical working conditions for Auger electron excitation were: primary electron beam current of approximately 20 nA and an electron energy of 10 keV. Depth profiles after sputtering with an argon ion beam (6 keV primary energy, impinging at an angle of 45° perpendicular to the sample surface) were analysed. The samples were fractured *in situ* to avoid any contamination.

Because of the high porosity (20–30%) of these fibre-reinforced ceramics their preparation for transmission electron microscopy (TEM) implies some serious problems during their cutting into slices in the μm range. To stabilize the specimens in a stepwise process under vacuum the material was first infiltrated with epoxy resin.

Thereafter, the thinning down to electron transparency was carried out by standard techniques including the cutting of thin ($< 150\,\mu$m) slices, mechanical grinding and finally ion milling (Ar, 6 kV). A further difficulty arises from the very different ion etching rates of fibre, matrix and interface layers, so that only a few parts of the specimens may finally be used. For investigating the general composite structure, especially the growth mode of the matrix between the different fibres in the weave, the high-voltage electron microscope (HVEM) JEOL-JEM 1000 operating at 1 MV was used, which allows a penetration up to the μm range. High-resolution electron microscope (HREM) images of the interface region between matrix and fibre were taken in the tilted illumination mode employing a JEM 100 C microscope operating at 100 kV. For details concerning the TEM investigation of ceramic materials see, for example, Refs 6 and 7.

Table 2. Density and porosity of the SiC-fibre and C-fibre reinforced SiC-composites

Reinforcing component	*Density* (g/cm^3)		*Porosity* (%)
	With coating	*Without coating*	
SiC-fibre	1·90	1·73	30
C-fibre	1·94	1·78	22

3 Results and Discussion

3.1 Measurements of microstructural data

The results of the density and porosity measurements are presented in Table 2. The apparent densities of the two composites are quite similar, although the SiC-fibre has a higher theoretical density relative to that of the C-fibre. This might be due to the fact that, on the one hand, the C-fibre bundles consist of 3000 fibres, whereas the SiC-fibre bundle consists of 500 fibres. On the other hand, the C-fibre diameter is about half the SiC-fibre diameter. These lead to a higher packing density of the C-fibre weave, resulting in a lower porosity of the composite. Furthermore, the density decreases with the SiC-coating being removed. The porosity is rather high, with different pore types being detected, as shown in Fig. 1. The well-defined structure of the weave is preserved for the C-fibre composite as can be recognized by a matrix layer around the bundle and by the fact that it was partly destroyed in the SiC-fibre material. Therefore, size and location of the pores are different in both composites. For the C-fibre reinforced material two pore types are evident (Fig. 1(a)):

—Interbundle pores: typically located at the fibre junction or between parallel fibre bundles ($< 3500\,\mu$m in length and $< 500\,\mu$m in width).
—Intrabundle pores: located between groups of fibres (length: 10–100 μm, width: 3–30 μm).

In addition, there are very small pores with sizes of around 1 μm × 1 μm located within a group of fibres. Such a distinction between intra- and interbundle pores is difficult to make for SiC-fibre reinforced materials (Fig. 1(b)) as the SiC-fibre bundles are not enclosed by a complete matrix material layer. Instead of this, individual fibres are coated with an SiC-layer. Usually, this fact indicates a high

(a)

(b)

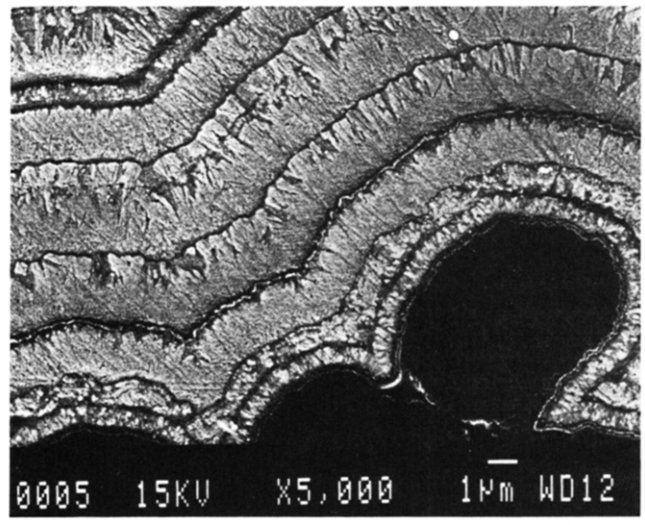

by high-resolution Auger electron spectroscopy and transmission electron microscopy before and after thermomechanical testing.

3.2.1 C-Fibre reinforced composite

Typical results of the HRAES investigation of the as-received state are presented in Figs 3 and 4. The secondary electron micrograph (Fig. 3(a)) shows the crossing of some fibre bundles with all the fibres of the perpendicular bundle being fractured. The transition region between a broken fibre bundle and the matrix was analysed to reveal the characteristic state of the individual components of the microstructure; the analytical results of five representative points (cf. Fig. 3(b)) in this transition region are demonstrated in Fig. 4(a)–(e). As can be seen, in the fibre only carbon could be analysed (Fig. 4(a)). The point analysis of the interface between fibre and matrix (Fig. 4(b)) revealed a carbon-rich layer containing a small amount of nitrogen and oxygen at the interface. Obviously, during the CVI process nitrogen diffuses to the interface and into the matrix. At the fracture surface of an individual matrix layer (Fig. 4(c)) no carbon enrichment was detected. However, a carbon enrichment was ascertained between the layers (Fig. 4(d)) which may enable the sliding of the inner matrix layer during fracture (cf. Fig. 5). Apparently, the corresponding reinforcing mechanism is not limited to a pull-out of the fibres, but includes the neighbouring matrix regions, thus influencing the mechanical properties. At the outermost matrix surface, carbon and small amounts of oxygen were detected (Fig. 4(e)).

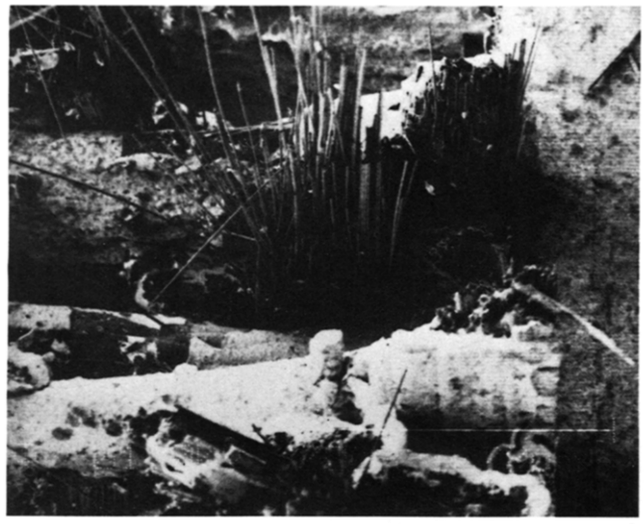

(a)

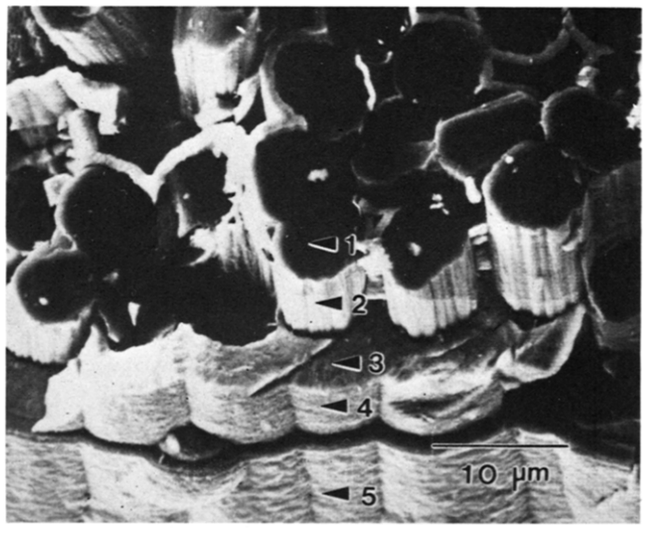

(b)

Fig. 3. Secondary electron micrographs (a) of the fracture surface and (b) with indication of the HRAES analysed points.

A more detailed and comprehensive illustration of the above results as well as some further important features concerning the microstructure of the fibre–matrix interface region are gained by transmission electron microscopy. Figure 5 reveals the structure of the CVI-grown SiC-matrix, clearly pointing out the dendritic growth of SiC (perpendicular to the fibre surface). The smaller stripe pattern within each dendrite can be identified as irregular sequences of stacking faults. They are mainly a result of the partial transformation from the cubic SiC to different hexagonal SiC-polytypes (about 20%, cf. Table 3). Furthermore, this figure shows the above-mentioned carbon layers oriented almost parallel to the fibre surface, separating individual matrix layers. Such carbon layers may enable sliding within the matrix to occur and can therefore influence the fracture process. Between the dendritic SiC-crystallites, i.e. in the growth direction, no carbon enrichment was detected.

Figure 6 demonstrates a cross-section of a C-fibre reinforced composite. The pores between the fibres as well as the thin matrix regions indicate the limitation of the infiltration process arising from the very compact fibre arrangement within the bundle, which in the composite prevents the precursor gas from distributing homogeneously. Moreover, as can be recognized in Fig. 7, thicker matrix regions (on the left) enclosing the whole fibre bundle can prevent the infiltration of the precursor gas if the growth rate of the matrix material outside the fibre bundle is much higher than inside the bundle. Higher magnifications of the interface between a carbon fibre and the dendritic SiC-matrix are shown in Fig. 8. In Fig. 8(a) the fibre (1) and the matrix (3) are separated by a 70-nm thick carbon layer (2). As this carbon layer contains several large pores and even empty channels, gases from the environment may reach the interface in a pipe-diffusion process. This may lead

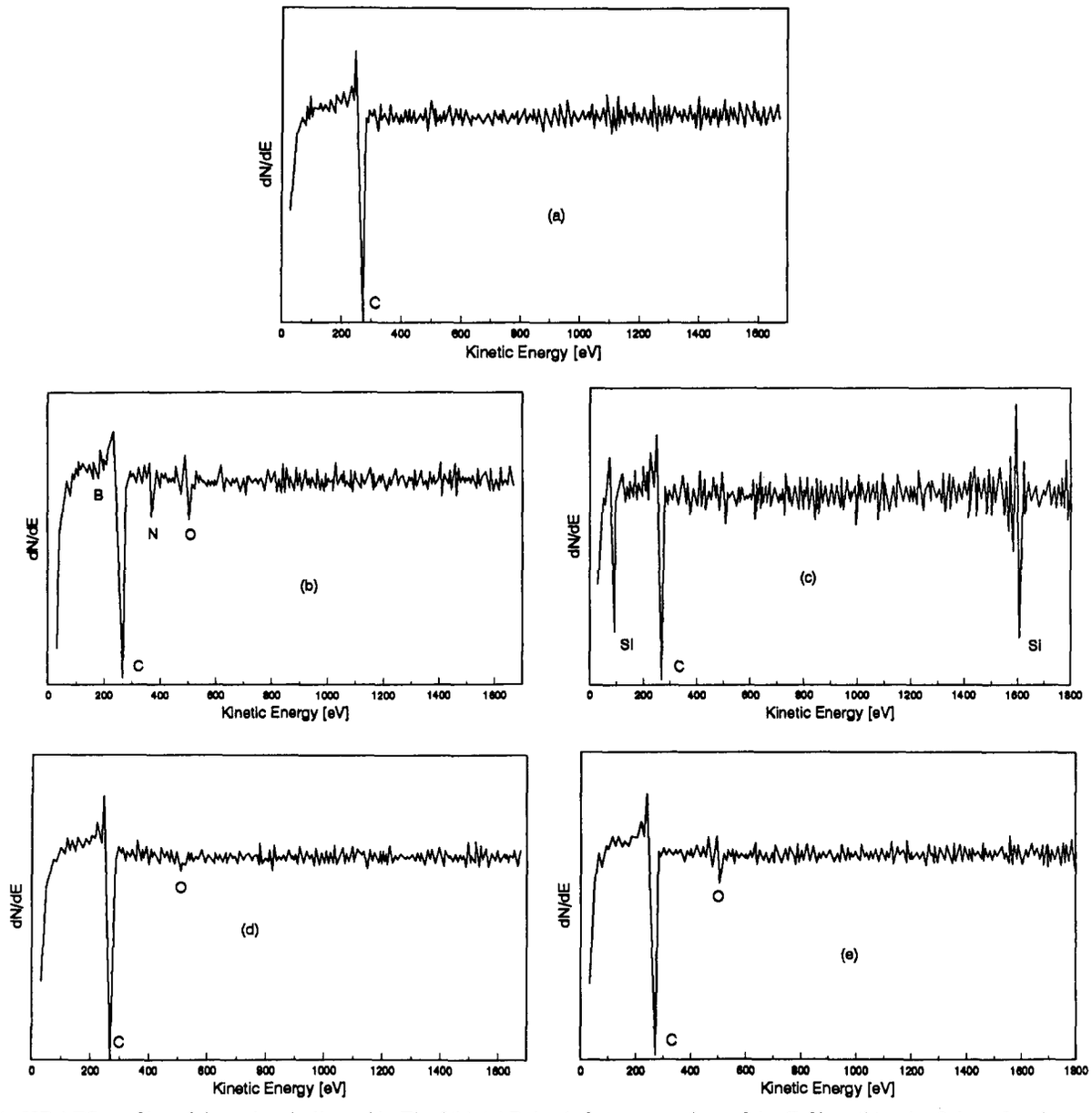

Fig. 4. HRAES profiles of the points indicated in Fig. 3(b): (a) Point 1: fracture surface of the C-fibre; (b) point 2: interface between fibre and matrix; (c) point 3: fracture surface of a matrix layer; (d) point 4: interface between two matrix layers; (e) point 5: surface of a fibre bundle layer.

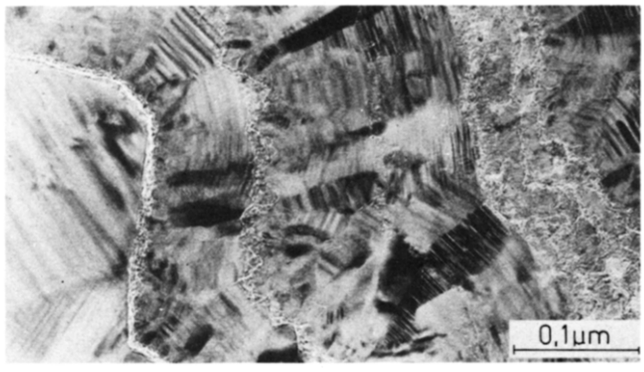

Fig. 5. Carbon interlayers in the SiC-matrix of the C-fibre composite.

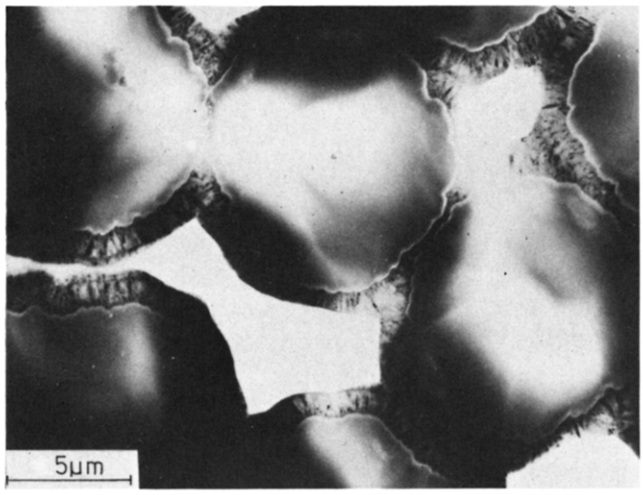

Fig. 6. TEM micrograph of a cross-sectioned C-fibre composite.

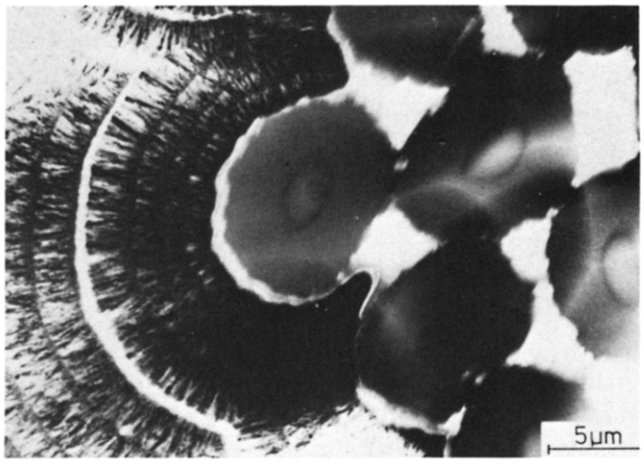

Fig. 7. C-fibre bundle, completely enclosed by the SiC-matrix.

to serious problems in high-temperature applications (cf. also Fig. 12). Figure 8(b) and (c) show the fibre, carbon layer and matrix structure as well as the attached interfaces taken by the lattice plane imaging technique. Both the lattice planes and the corresponding diffraction pattern indicate a turbostratic orientation of the basic graphite planes within the fibre parallel to its surface (cf. Fig. 8(c)).

In contrast, the carbon interlayer consists of small (8–10 nm), irregularly oriented graphite crystals and is possibly due to the fibre coating prior to the matrix infiltration process. On the very fibre surface (cf. the middle part of Fig. 8(c)) a nearly 10-nm thick well-developed graphite layer was found. Along its weakly bonded basic lattice planes the crack propagation is favoured, and so is a debonding process between fibre and matrix.

After three-point bending tests at elevated temperatures under vacuum HRAES and TEM did not reveal any influence of the heat treatment on the microstructure. As Fig. 9 demonstrates, the same interface structure (fibre/interlayer/matrix) was found as in untreated material. Especially the thin graphite layer at the fibre surface and the graphite crystals in the interlayer (indicated by arrows) are not influenced (cf. also Fig. 8(c)). This observation is in agreement with the results of the bending tests at high temperatures (cf. Fig. 14(a)).

3.2.2 SiC-Fibre reinforced composite

The HRAES investigation of the composite in the as-received state is demonstrated in Fig. 10. Using argon ion sputtering a tapered section of the interface between the fibre and matrix was generated *in situ*. Figure 10 shows that the interface between fibre and matrix is built up by layers differing in their chemical composition. In these layers only the elements C, Si and O were detected. Therefore the

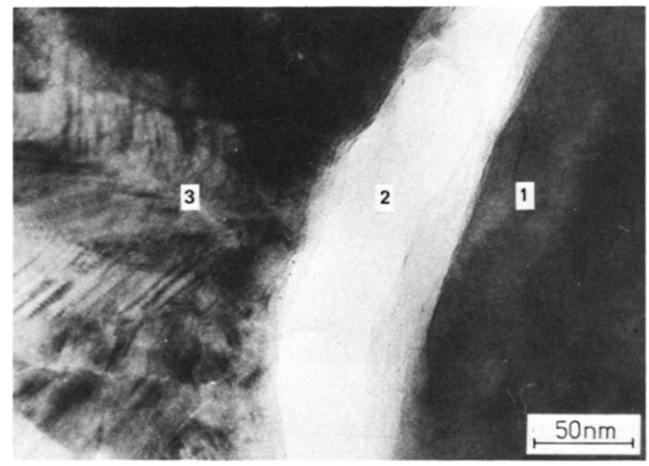

(a)

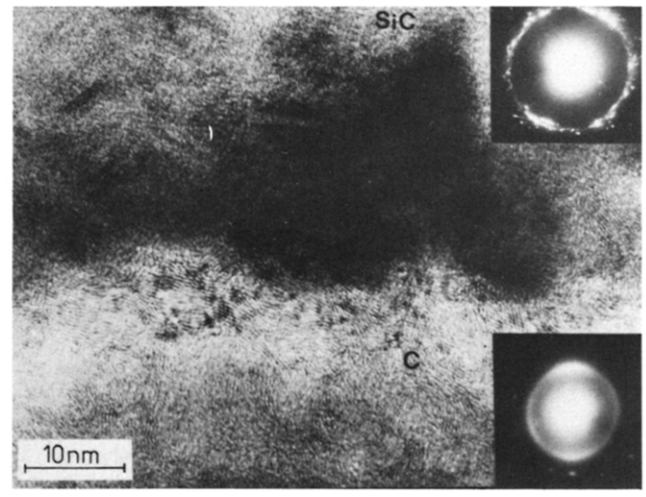

(b)

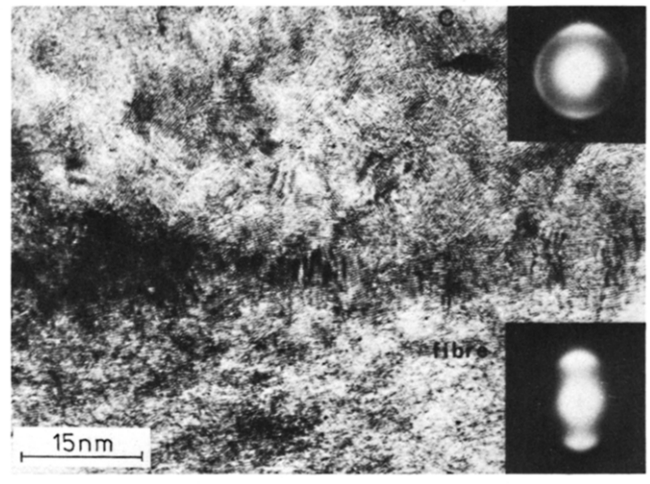

(c)

Fig. 8. (a) Carbon interface layer (2) in C-fibre (1) reinforced SiC (3); (b) HREM-image of the interfacial region between (3) and (2) in Fig. 8(a); (c) HREM-image of the interfacial region between (1) and (2) in Fig. 8(a).

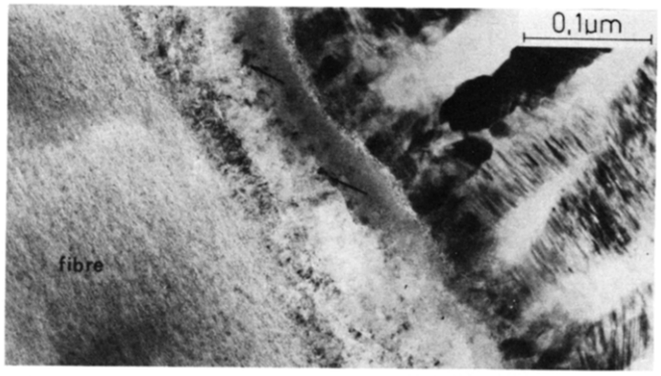

Fig. 9. Graphite particles (indicated by arrows) in the carbon layer of a C-fibre composite after three-point bending at 1300°C under vacuum.

line scans of these elements (Fig. 10(d)) from point 1 to point 2 (Fig. 10(c)) manifest the layered structure of the interface in the following sequence: fibre/C-rich layer/Si-O-layer/C-layer/SiC-matrix.

The TEM image (Fig. 11(a)) excellently confirms the interlayer sequence shown by HRAES. Between the two carbon layers (2) and (4) glassy material is embedded. During fibre debonding the crack propagates between the glassy layer (3) and the outermost carbon layer (4), with a very porous region being displayed. Fig. 11(b) shows the lattice plane image of the interface between the SiC-fibre ((1) in Fig. 11(a)) and the innermost carbon layer ((2) in Fig. 11(a)), whereas Fig. 11(c) reveals the interface

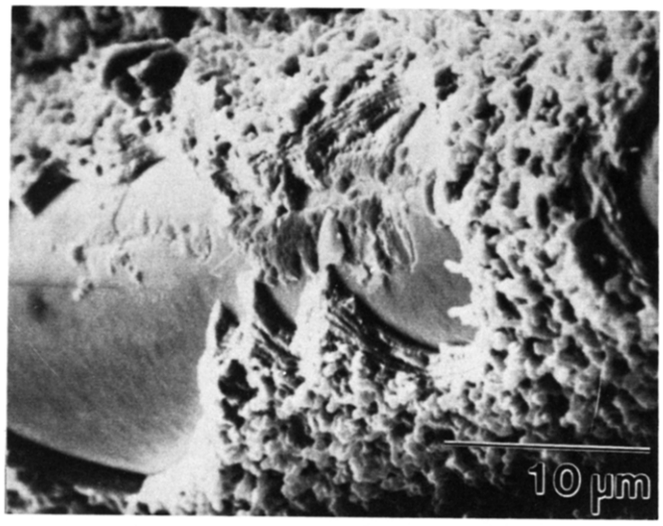

(a)

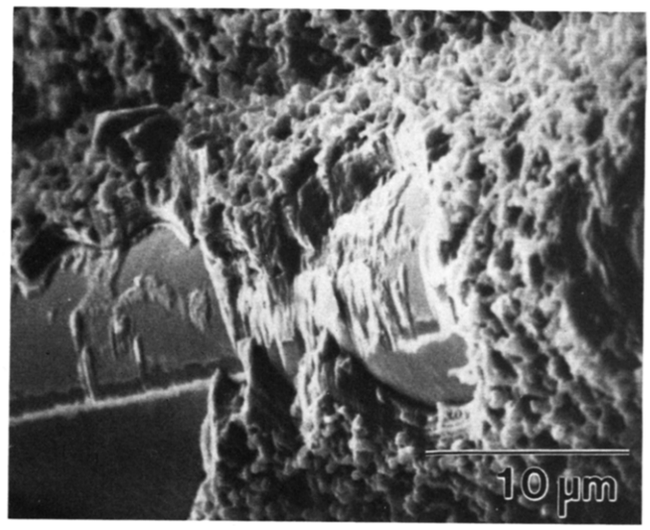

(b)

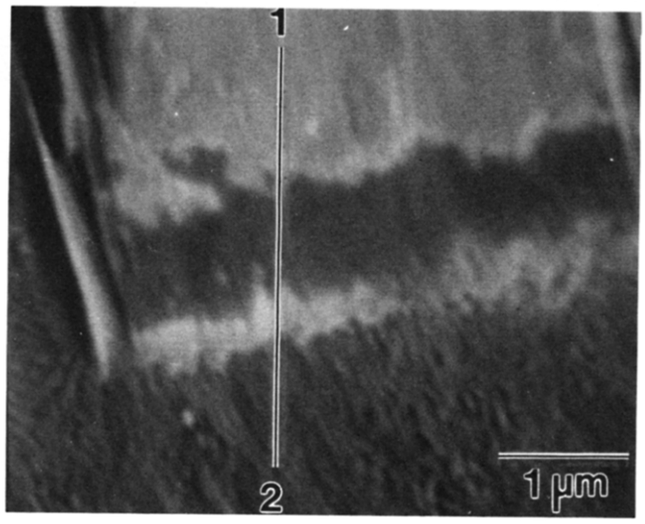

(c)

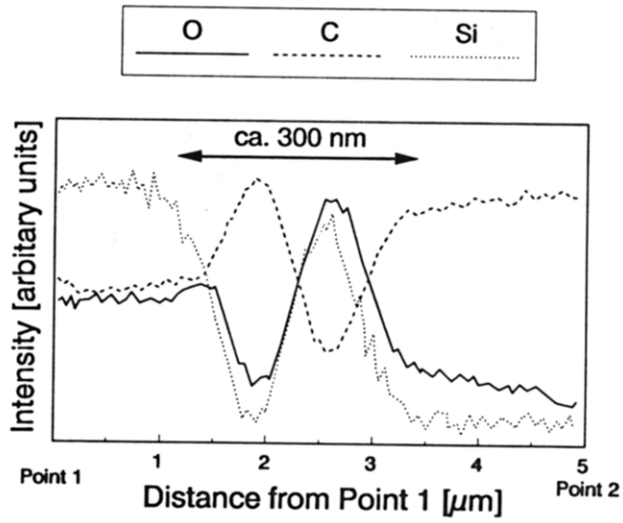

(d)

Fig. 10. HRAES investigation of the in-situ fractured SiC-fibre reinforced composite. (a) Secondary electron micrograph of the fracture surface; (b) as in (a) after etching with Ar ions; (c) secondary electron micrograph of the interface fibre–matrix after etching with Ar ions indicating line scan along 1 to 2; (d) line scan profiles of C, Si and O along 1 to 2 indicated in Fig. 10(c).

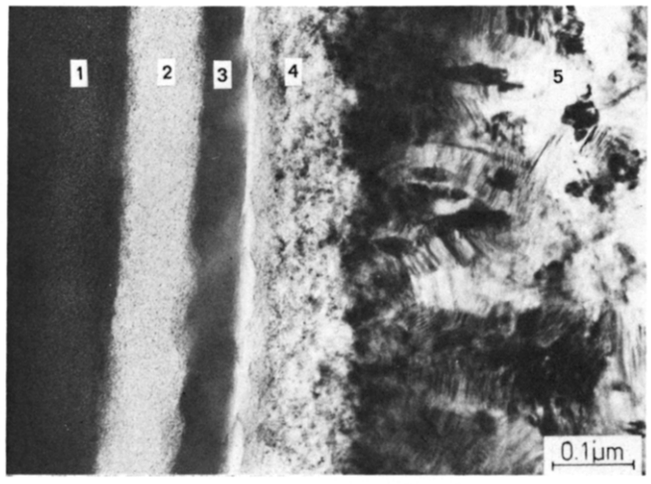

(a)

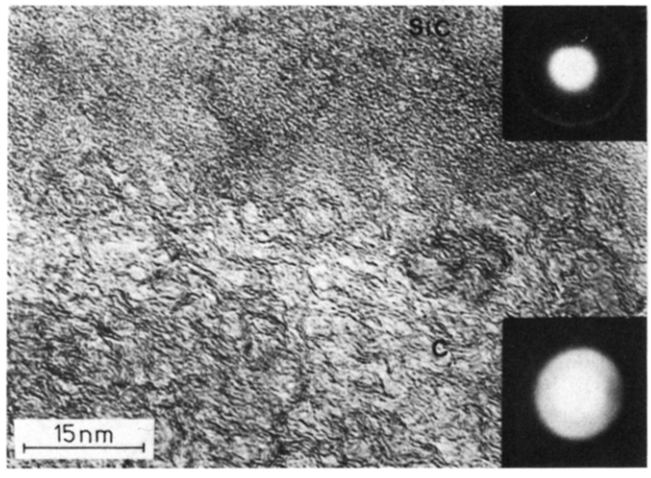

(b)

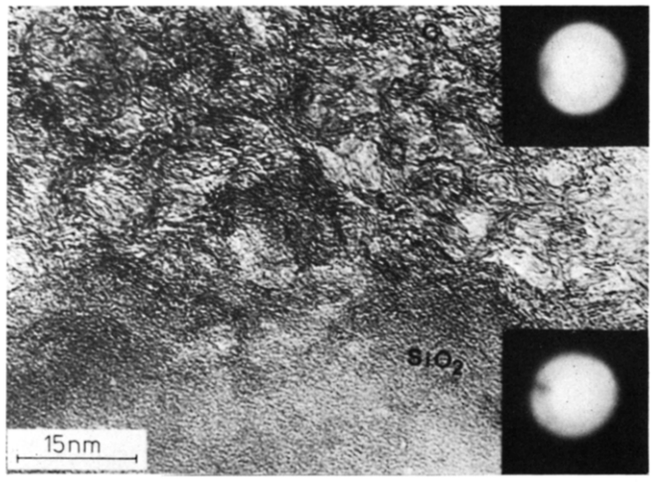

(c)

Fig. 11. (a) Layered interface in SiC-fibre (1) reinforced SiC (5), carbon layer (2), SiO_2-layer (3), carbon layer due to coating (4); (b) HREM-image of the interfacial region between (1) and (2) in Fig. 11(a); (c) HREM-image of the interfacial region between (2) and (3) in Fig. 11(a).

between this carbon layer and the glassy region ((3) in Fig. 11(a)). Unlike carbon fibre-reinforced composite (cf. Fig. 8(c)) the carbon interlayer (2) does not consist of small graphite crystallites in SiC-fibre containing materials. As can be seen in Fig. 11(c) (top) a cellular structure of irregularly distributed atomic planes of graphite has been identified. This feature as well as the rough and diffuse interfaces to the neighbouring SiC-fibres and the glassy layer allow the conclusion to be drawn that the carbon layer (2) in SiC-fibre reinforced material results from a chemical reaction. Following Ref. 18, surface oxidation on SiC-fibres releases carbon and silicon oxide, thus being responsible for the formation of the interlayers (2) and (3) in the composite under investigation. The second carbon layer (4) is supposed to be built up at the beginning of the matrix infiltration process.

The use of SiC-fibres (Nicalon) is associated with layered interfaces in composites with glassy[19,20] as well as ceramic matrices.[21] These results are also in agreement with thermodynamic calculations.[22]

There is a change in structure and composition of the interface when the composite is tested at high temperatures (1000 to 1300°C) in air, with both the interface and the SiC-matrix oxidizing. The principal mechanism causing the interfacial oxidation is due to pipeline oxidation. The C-layer reacts with the oxygen, thus forming cavities in the interfaces. Therefore, as is indicated in Fig. 12, the fibre surface is then in an oxidized state, too, as manifested by the formation of two glassy layers in the transition region. After testing under vacuum there was again no composite degradation.

3.3 Mechanical properties

3.3.1 Tensile tests at room temperature

Linear stress–strain behaviour was observed in both materials until the first matrix cracking occurred at a

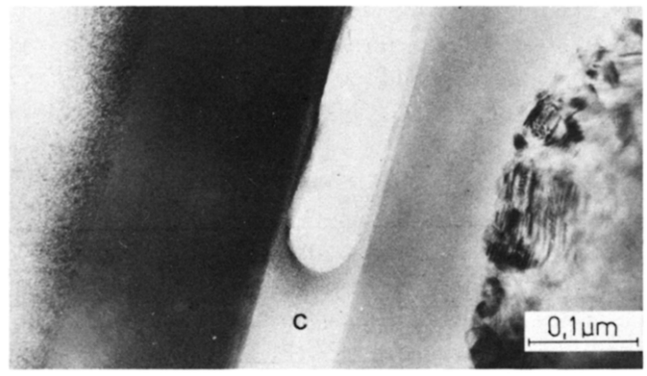

Fig. 12. Cavities in the carbon interlayer after high-temperature treatment of the SiC-fibre composite in air.

similar stress level of about 40 MPa. Thus, both composites respond to this initial loading in the same way. Above this stress level the stress–strain curves of the two materials are different. Up to the ultimate strength of the composite the SiC-fibre reinforced composite shows a linear behaviour. The upper part of the curve is characterized by a slightly reduced slope. In contrast to this the C-fibre reinforced composite shows a non-linear behaviour which is due to the formation of multiple matrix cracks. The ultimate strength of the SiC-fibre reinforced material ($\sigma_{UTS} = 120$ MPa) is about twice the ultimate strength of the C-fibre reinforced material ($\sigma_{UTS} = 63$ MPa). It seems to be possible that load transfer is more effective in the SiC-fibre material. This could be due to the fact that in the SiC-fibre material each fibre is coated by a matrix layer whereas in the C-fibre material the coating of each fibre is not realized. Obviously, the moderate strength and the observed stiffness reveal that the potential of high strength reinforcing fibres in a SiC-matrix has not been fully realized which is partly due to the extended defects in these microstructures.

Using intermittent tests the damage process was investigated. The different behaviour of the two composites is reflected by the damage area covering up to about 13 mm in the SiC-fibre material in contrast to about 5 mm in the C-fibre material (Fig. 13). In both materials the damage was initiated at the specimen surface with the breakage of the outer fabric weaves. Higher stressing of the SiC-fibre reinforced material causes cracking parallel to the fabric weave.

Delamination as well as detachment of the SiC-fibre bundles takes place. Most of the cracks parallel to the SiC-fibres are observed when reaching the tensile strength of the composite. This intensive crack branching could not be seen in the case of the C-fibre reinforced material. Here, the main damage mechanism is delamination so that the load transfer is caused by shear stress and/or by tensile opening stresses at the tip of a crack. Fragments of the matrix layers, being characteristic for the observed matrix microstructure, could be seen on the fracture surface for both composites.

3.3.2 Bending tests at room and elevated temperatures

The stress–strain curves at different temperatures are represented in Fig. 14. As is generally the case in ceramics, the strength determined in the bending tests is higher than that in the tensile tests. In each case, the first part of the loading procedure leads to a continuous increase of stress and strain until the maximum stress is reached; no distinct bend-over stress was observed, which indicates that crack initiation does not play a dominating role during initial loading. However, a dramatic drop of the stress at maximum load signifies the relatively brittle behaviour of these composites. Only SiC-fibre reinforced SiC tested at room temperature is able to withstand increasing stress again after having passed the point of maximum load.

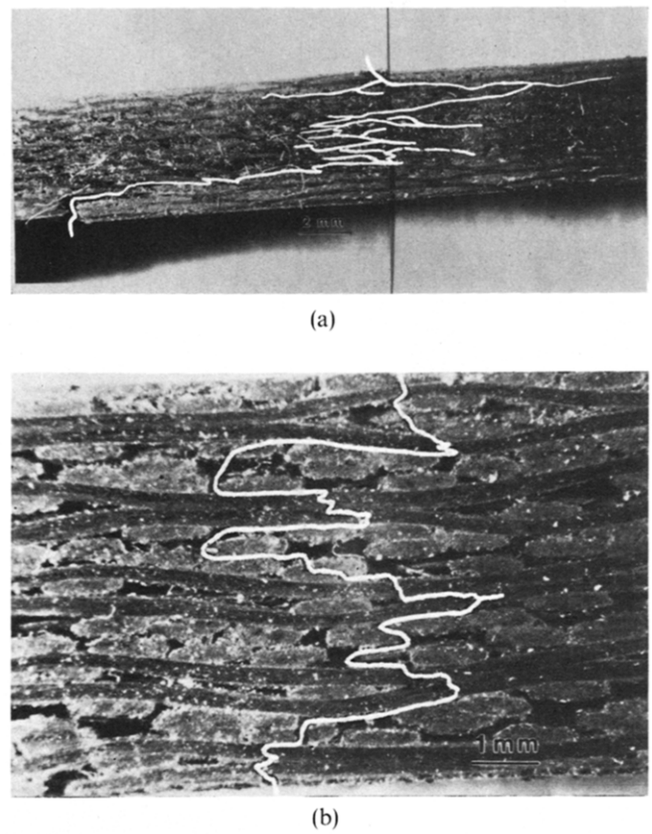

Fig. 13. Reflected light micrographs of the SiC-fibre (a) and C-fibre (b) reinforced composites, showing the extension of the damaged specimen volume in room-temperature tensile tests.

Testing at elevated temperatures under vacuum revealed an increase in strength and Young's modulus with increasing temperature in the case of the C-fibre reinforced composite. In contrast to this a strong decrease of strength (20–30% of the room-temperature value) and Young's modulus was observed for the SiC-fibre/SiC-composite when being tested at high temperatures in air. These results contradict the data of Lamicq *et al.*,[4] who found a slight increase in strength up to 1300°C for a SiC/SiC-composite. On the other hand, there is a good agreement with the findings of Caputo *et al.*,[23] who also measured a decrease in strength with increasing temperature when testing an SiC(Nicalon)/SiC-composite in air. The increase in strength of C-fibre reinforced materials is also described in the literature.[24]

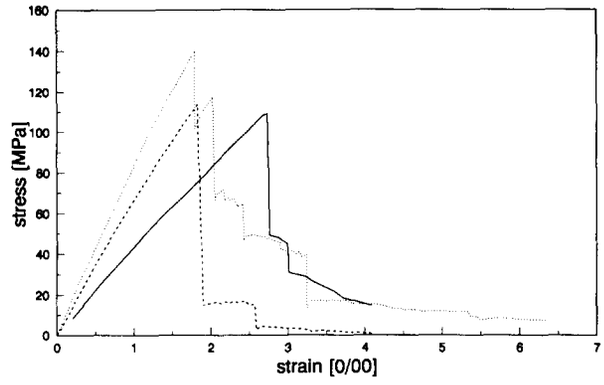

(a)

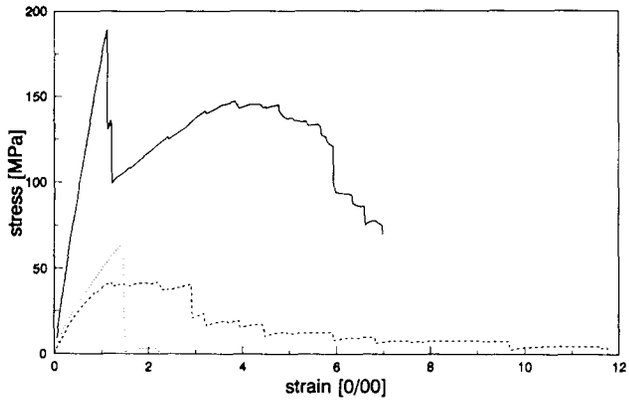

(b)

Fig. 14. Stress–strain curves (three-point bending) at room temperature (——) and elevated temperatures (– – –, 1000° C; ·····, 1300° C) of (a) the C-fibre (tested in vacuum) and (b) the SiC-fibre reinforced composite (tested in air).

In order to clarify the damage process a few specimens were polished on two sides prior to testing. Then the stress was increased in approximately 10 MPa steps and the specimens were investigated after each step. In both materials, the damage process was initiated at the outermost surface starting from a flaw in the SiC-coating. Then the leading crack propagated through the outermost fibre bundle and was deflected along the fibre–matrix interface.

In the case of the SiC-fibre reinforced material, subsequent detachment between the bundles orientated perpendicular and parallel to the rollers of the bending fixture took place. Finally, a crack was generated in the centre of the specimen running throughout the sample in a perpendicular direction to loading (interlaminar). This caused a stepwise decrease of the stress–strain curve. The nature of this crack led to the conclusion that shear stresses were responsible for final failure, since the shear stress reaches its maximum on the neutral axis. Although the span to height ratio was as large as possible, this ratio should have been higher in order to further reduce the shear stress of these materials.

In the C-fibre material a different behaviour was observed. The crack propagated from the parallel fibre bundle into the bundle perpendicular to the applied stress. In most cases the bundle breakage was brittle. Only little pull-out could be detected. Delamination took place throughout the samples with cracks under 45 degree orientation to the loading direction. This again indicates noticeable shear stresses in the centre of the specimens.

4 Summary

The microstructures of both investigated composites are characterized by relatively high porosities and a layered structure of the matrix. However, the chemical vapour infiltration process is shown to proceed in different ways in these composites: A complete matrix layer around a fibre bundle is easier to form in the C-fibre reinforced composite than in the SiC-fibre material, which is explained by the higher packing density, caused by the higher numbers of fibres per bundle and the smaller fibre diameter in the C-fibre reinforced composite.

The matrix of the C-fibre reinforced composites contains carbon layers oriented nearly parallel to the fibre surface. Thus, the energy dissipative micromechanics are not limited to the pull-out of the fibres but also include the neighbouring matrix regions. In the case of the SiC-fibre reinforced material a more complicated interlayer structure has been formed between the matrix and the fibre during the CVI process; a silicon oxide layer is located between two amorphous carbon regions.

The damage process is always initiated at surface flaws. Main processes are cracking in the interlaminar (delamination) and intralaminar mode (detaching of fibre bundles). Debonding was proved to take place in the C-layer adjacent to the matrix. Therefore, pull-out is concentrated in this layer. During fibre debonding cracks easily form between the glassy and the outermost carbon layer, leading to the intensive crack branching observed in this material.

On the other hand, these C-layers will be destroyed when these composites are used in air at elevated temperatures. Oxidation, probably mainly pipeline oxidation, takes place, leading to the degradation of the interfaces with the effect of strength reduction. Contrary to that, an increase in strength was observed when the C-fibre reinforced material was tested under vacuum at elevated temperatures. Obviously, the load transfer is more effective at higher temperatures and the effect of

thermal residual stresses is diminished when the test temperature approaches the processing temperature. In addition, microstructural and microanalytical investigations revealed that no severe changes of the state of the interfaces occurred during thermomechanical testing under vacuum.

In summary, these results show that the interaction of fibre and matrix controls the mechanical properties of the composite. With respect to the specific processing route of the composites examined in this study the application temperature will often be higher than the processing temperature, leading to different thermal stresses compared to room-temperature applications. The mechanical behaviour will be strongly affected by this fact. Furthermore, the fibre and matrix degradation due to high-temperature reactions, i.e. oxidation, will lower the relevant mechanical properties.

References

1. Meier, B., Spelman, D. & Grathwohl, G., Microstructure, interfaces and mechanical properties of fibre-reinforced glasses. In *The Fourth European Conference on Composites Materials*, Stuttgart, FRG, ed. J. Füller, G. Grüninger, K. Schulte, A. R. Bunsell and A. Massiah, 25–28 September 1990. Elsevier Applied Science, London and New York, 1990, pp. 475–90.
2. Prewo, K. M. & Brennan, J. J., High strength silicon carbide fibre-reinforced glass-matrix composites. *J. Mat. Sci.*, **15** (1980) 463–80.
3. Caputo, A. J., Lowden, R. A. & Stinton, D. P., Fibre-reinforced ceramic composites made by chemical vapour infiltration. Oak Ridge Nat. lab., Contract No. AC05-840R21400, Report No. DE 85 015587, 1985.
4. Lamicq, P. J., Bernhart, G. A., Dauchier, M. M. & Macc, J. G., SiC/SiC composite ceramics, *Am. Cer. Soc. Bull.*, **65**(2) (1986) 336–8.
5. DIN 51056, Prüfung keramischer Roh- und Werkstoffe: Bestimmung der Wasseraufnahme und der offenen Porosität.
6. Pippel, E. & Woltersdorf, J., High-voltage and high-resolution electron microscopy studies of interfaces in zirconia-toughened alumina. *Phil. Mag. A*, **56** (1987) 595–613.
7. Woltersdorf, J. & Pippel, E., The structure of interfaces in high-tech ceramics. *Coll. de Physique C1, Suppl. 1*, **51** (1990) C1–847.
8. Wahl, G., Chemische Abscheidung aus der Gasphase. In *Proceedings Verbundwerk*. Demat Exposition Managing, Frankfurt (Main), PF 110611, 1988.
9. Murakami, T., Die Gefügebestandteile von Eisen–Chrom–Kohlenstofflegierungen. *Stahl und Eisen*, **40** (1920) 988.
10. Weiss, J. R. & Diefendorf, R. J., Chemically vapour deposited SiC for high temperature and structural applications. In *Silicon carbide—1973*, ed. R. C. Marshall, J. W. Faust Jr, C. E. Ryan. University of South Carolina Press, Columbia, South Carolina, 1973, pp. 80–91.
11. Moeller, H. H., Long, W. G., Caputo, A. J. & Lowden, R. A., Fibre-reinforced ceramic composites. *Cer. Eng. Sci. Proc.*, **8**(7–8) (1987) 977–84.
12. Brennfleck, K. & Porsch, G., Chemische Gasphasenabscheidung von SiC auf Graphitsubstrate für Anwendungen in der Halbleiterindustrie. SNO, Schunk Nukem Oberflächentechnik, W-6400 Gießen, FRG.
13. Hsueh, C.-H. & Becher, P. F., Thermal expansion coefficients of unidirectional fiber-reinforced ceramics. *J. Am. Cer. Soc.*, **71**(10) (1988) C-438–C-144, and corrections *J. Am. Cer. Soc.*, **72**(3) (1989) C-359.
14. Brändle, M., Diploma thesis, Institut für Werkstoffkunde II, Universität Karlsruhe, 1991.
15. Ruska, J., Gauckler, L. J., Lorenz, J. & Rexer, H. U., The quantitative calculations of SiC-polytypes from measurements of X-ray diffraction peak intensities. *J. Mat. Sci.*, **14** (1979) 2013–17.
16. Böder, H., Gölden, D., Rose, P. & Würmseher, H., Herstellung von Kohlenstoffasern. *Z. Werkstofftechnik*, **11** (1980) 275–81.
17. Knippenberg, W. F., Growth phenomena in silicon carbide. *Philips Research Reports*, **18** (1963) 161–274.
18. Cooper, R. F. & Chyung, K., Structure and chemistry of fibre–matrix interfaces in silicon carbide fibre-reinforced glass–ceramic composites, an electron microscopy study. *J. Mat. Sci.*, **22** (1987) 3148–60.
19. Meier, B. & Grathwohl, G., Microanalytical investigations of fibre-reinforced ceramic materials. *Fresenius Z. Anal. Chem.*, **333** (1989) 388.
20. Chaim, R. & Heuer, A. M., The interface between (Nicalon) SiC-fibres and a glass–ceramic matrix. *Adv. Cer. Mat.*, **2** (1987) 154–8.
21. Brennan, J. J., Interfacial studies of chemical vapour infiltrated (CVI) ceramic matrix composites. United Technology Research Center, East Hartford, Connecticut, USA, Annual report, Contract-N60014-87-C-0699, 1988.
22. Greil, P., Thermodynamic calculations of Si–C–O fibre stability in ceramic matrix composites. *J. Eur. Cer. Soc.*, **6** (1990) 53–64.
23. Caputo, A. J., Stinton, D. P., Lowden, R. A. & Besmann, Th. M., Fibre-reinforced SiC composite with improved mechanical properties, Oak Ridge Nat. Lab. *Am. Cer. Soc. Bull.*, **66**(2) (1987) 368.
24. Nakano, K., Hiroyuki, A. & Ogawa, K., Carbon fibre-reinforced silicon carbide composites. In *Developments in the Science and Technology of Composite Materials, ECCM-4*, Stuttgart, FRG, 25–28 September, 1990, ed. J. Füller, G. Grüninger, K. Schulte, A. R. Bunsell & A. Massiah, Elsevier Applied Science, London and New York, 1990, pp. 419–24.